Title	Effect evaluation of drainage condition and water content on cyclic plastic deformation of aged ballast and its estimation models
Author(s)	Yang, Jiaqiang; Ishikawa, Tatsuya; Tokoro, Tetsuya; Nakamura, Takahisa; Kijiya, Ippei; Okayasu, Takashi
Citation	Transportation geotechnics, 30, 100606 https://doi.org/10.1016/j.trgeo.2021.100606
Issue Date	2021-09
Doc URL	http://hdl.handle.net/2115/89861
Rights	© <2021>. This manuscript version is made available under the CC-BY-NC-ND 4.0 license http://creativecommons.org/licenses/by-nc-nd/4.0/
Rights(URL)	http://creativecommons.org/licenses/by-nc-nd/4.0/
Type	article (author version)
File Information	Revised_Manuscript.pdf

Effect evaluation of drainage condition and water content on cyclic plastic deformation of aged ballast and its estimation models

Jiaqiang Yang [i], Tatsuya Ishikawa [ii], Tetsuya Tokoro [iii], Takahisa Nakamura [iv] and Ippei Kijiya [iv], Takashi Okayasu [v]

[i] **Jiaqiang Yang, Doctor Course Student**

Graduate School of Engineering, Hokkaido University, Kita 13, Nishi 8, Kita-ku, Sapporo 060-8628, Japan

e-mail: jq-yang@eis.hokudai.ac.jp

[ii] **Tatsuya Ishikawa, Professor** (*Corresponding author*)

Faculty of Engineering, Hokkaido University, Kita 13, Nishi 8, Kita-ku, Sapporo 060-8628, Japan

e-mail: t-ishika@eng.hokudai.ac.jp

[iii] **Tetsuya Tokoro, Associate Professor**

Faculty of Engineering, Hokkai-Gakuen University, 1-1, Minami 26, Nishi 11, Chuo-ku, Sapporo 064-0926, Japan

e-mail: tokoro@cvl.hokkai-s-u.ac.jp

[iv] **Takahisa Nakamura, Ph.D.**

Track Technology Division, Railway Technical Research Institute, 2-8-38, Hikari-cho, Kokubunji 185-8540, Japan

e-mail: nakamura.takahisa.19@rtri.or.jp

[iv] **Ippei Kijiya, Mr.**

Track Technology Division, Railway Technical Research Institute, 2-8-38, Hikari-cho, Kokubunji 185-8540, Japan

e-mail: kijiya.ippei.83@rtri.or.jp

[V] **Takashi Okayasu, Associate Professor**

Faculty of Agriculture, Kyushu University, 6-10-1, Hakozaki, Higashi-ku, Fukuoka 812-8581, Japan

e-mail: okayasu@bpes.kyushu-u.ac.jp

Abstract

With the ballast aging, the changes in the size and shape of the ballast particle reduce the drainage capacity, as well as cause a greater permanent deformation of the railroad ballast. Therefore, it is meaningful to investigate the effect of aging on the mechanical behavior of unsaturated ballast, and to estimate the cyclic plastic deformation by considering the aging effects. Here, "aging effect" means the increase in fine fraction content and the particle shape becomes rounded and smooth as compared with fresh ballast. In this study, the influence of aging on the cyclic plastic deformation of unsaturated ballast was evaluated through a series of cyclic loading triaxial compression tests. Test results indicate that the cyclic plastic deformation of ballast is seriously affected by water content, fine fraction content and drainage condition, and the increasing trend becomes more remarkable at the water-rich aged ballast under the fully undrained condition since the effective confining pressure decreases due to the generation of excess pore water pressure. Furthermore, the applicability of two types of estimation models (i.e., a semi-empirical model named University of Illinois at Urbana-Champaign (UIUC) model, and an elasto-plastic model named subloading surface extension (SSE) model) to the prediction for cyclic plastic deformation of unsaturated ballast is also verified in this study by comparing with results of cyclic loading triaxial compression tests. As the result, it is revealed that the UIUC model is suitable for predicting the cyclic plastic deformation of fresh ballast (or slightly aged ballast) with different water contents under the fully drained condition, and the SSE model shows good potential to estimate the cyclic plastic deformation of fresh and aged ballasts by considering the effects of water content and drainage condition. The findings of this study indicate that drainage conditions have a significant effect on predicting the cyclic plastic deformation of aged ballast, and appropriate test conditions for triaxial compression tests (i.e., CD and CU tests) should be selected according to hydraulic properties (i.e., permeability and water retentivity) of the aged ballast.

Keywords: Aged ballast; Unsaturated soil; Cyclic plastic deformation; Laboratory element test; Estimation models.

1 Introduction

The ballasted track structure (Fig. 1) is one of the typical track structures for traditional railways in Japan. As passing tonnage of trains accumulates, clean or fresh ballast might be gradually contaminated with fouling materials, which are finer than fresh ballast aggregates, due to the ballast abrasion, breakdown, and external contamination (Indraratna et al., 2011; Selig and Waters, 1994). Selig and Waters (1994) pointed out that ballast fouling is mainly due to the degradation of ballast particle size and shape, which is called "aging" in this study. It is worth noting that the definition of "aging" used in this study is different from the definition of "fouling" commonly used in most previous studies. The aged ballast considers the changes in ballast particle size and shape, while the fouled ballast does not consider the change in particle shape. Some past studies indicated that the ballast fouling will cause a greater permanent deformation of ballasted tracks (Ebrahimi et al., 2015; Indraratna et al., 2013a; Ishikawa et al., 2019). In addition, the increase in fine fraction content caused by ballast fouling or aging affects the permeability and water retentivity of the ballast, which may cause an increase in water content of the ballasted layer and further increase the cyclic plastic deformation of the ballasted track (Indraratna et al. 2010; Tennakoon et al., 2012). The current Japanese design standard (RTRI, 2012) adopts a semi-empirical formula to estimate the cyclic plastic deformation of ballast for the construction of new lines. However, this formula cannot separately consider the adverse effects of water content and aging on the cyclic plastic deformation of the ballast.

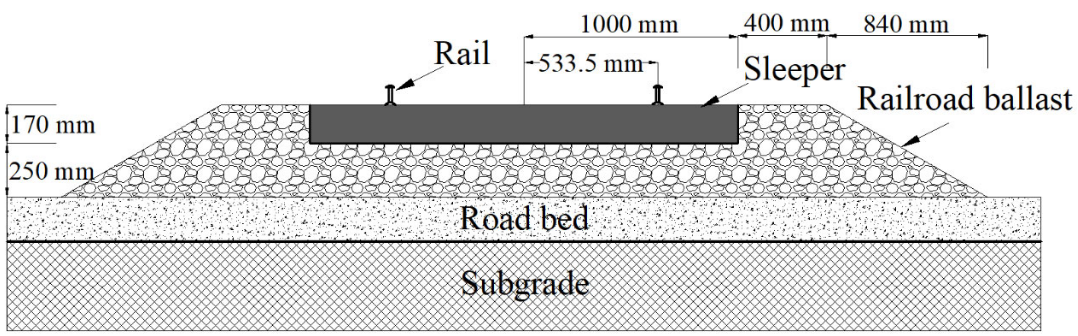

Fig. 1. Schematic diagram of a typical ballasted track structure in Japan.

For cyclic triaxial tests, previous studies indicated that the cyclic plastic deformation of the aggregate materials is affected by the stress level, water content, fine fraction content, grading (Lekarp et al., 2000; Le Pen et al., 2013). For example, the increase in fine fraction content seriously alters the deformation-strength characteristics of the ballast, depending on the amount of fouling materials mixed with clean ballast (Dareeju et al., 2015; Lackenby et al., 2007). Besides, Indraratna et al. (2013a) pointed out that with the increase in the fine fraction content, the sleeper settlement of fouled ballasted track increases. Ebrahimi et al. (2015) indicated that the water content of fouling materials has a significant effect on accelerating the cyclic plastic deformation and changing the shape of deformational behavior of ballast from a small rate of plastic deformation to a high rate of plastic deformation. Ishikawa et al. (2019) revealed that both water content and fine fraction content may have serious influences on cyclic plastic deformation of the ballast. However, the effects of particle shape changes and drainage conditions on cyclic plastic deformation have not been evaluated in previous studies on fouled ballast so far.

For the semi-empirical model, many advanced phenomenological models (e.g., Abadi et al., 2016; Lekarp et al., 2000; Monismith et al., 1975) for estimating the accumulative strain of geomaterials under cyclic loading have been proposed by past researchers. In these models, the UIUC model is a simple model to predict the cyclic plastic deformation of pavements under repeated traffic loads, because its input parameters can be easily calculated by the shear strength parameters based on the monotonic triaxial test or the direct shear test instead of the cyclic triaxial test (Chow et al., 2014a, 2014b; Qamhia et al., 2016). After that, the applicability of the UIUC model was also verified for clean and fouled ballasts with different water contents and fine fraction contents (Ishikawa et al., 2019). However, the applicability of this model to the prediction for the cyclic plastic deformation of aged ballast has not been verified so far by considering the effect of drainage condition. On the other hand, various constitutive models for granular materials have been developed so far (Hashiguchi and Ueno, 1977; Habiballah and Chazallon, 2005; Iwan, 1967; Mroz et al., 1981; Niemunis et al., 2005). In these models, the subloading surface model shows a good ability to predict the cyclic plastic deformation behavior for metals and clay (Hashiguchi and Ueno, 1977). After that, this model was modified by assuming an existence of the elastic domain surface inside the subloading surface to realistically describe the inelastic deformation behavior of coarse granular material under cyclic loading conditions. The validity of SSE model in predicting the permanent deformation of air-dried clean ballast under cyclic loading was verified by comparing the test results with the numerical results (Okayasu et al., 2014). However, the applicability of this model to predict the cyclic plastic deformation of the aged ballast with various water contents and drainage conditions has not been discussed so far.

To improve the track structure design and reduce maintenance costs, the main objective of this study is to comprehensively investigate the effect of aging which includes changes in particle shape and particle size on the cyclic plastic deformation of unsaturated ballast, and to estimate the cyclic plastic deformation of unsaturated ballast by considering the aging effects. For these purposes, this study first evaluates the influence of aging on cyclic plastic deformation of unsaturated ballast through a series of suction-controlled cyclic loading triaxial compression tests for fresh and aged ballast. After that, the applicability of two types of estimation models (i.e., UIUC model and SSE model) is verified to the prediction for the cyclic plastic deformation of fresh and aged ballast with various water contents and drainage conditions.

2 Test materials

In general, most of the Japanese railroad ballasts are composed of angular, crushed, and hard andesite stone. The grain size distribution of properly graded ballast in the Japanese railway standard ranges from 19 to 63 mm. Fresh ballast or called clean ballast (CB) and aged ballast (AB) are used as test materials. In Fig. 2, the terms "1/1CB" and "1/1AB" refer to the full-scale fresh ballast and full-scale aged ballast obtained from actual railway tracks in Japan. Here, 1/1AB (Fig. 2) was extracted from heavily aged railway tracks. It should be noted that field investigations on aged railway tracks in Japan show that the fine fraction content (F_c) of in-situ aged ballast is generally between 0 and 15%. Therefore, the maximum F_c value of 15% in the field investigation is used as the basis for the laboratory test condition. However, in this study, the small-scale fresh ballast (1/2CB) and the small-scale aged ballast (1/2AB) were employed as test samples due to the specimen size in the medium-size triaxial apparatus. Both 1/2CB and 1/2AB have the half mean grain size of 1/1CB and 1/1AB with a parallel gradation (Fig. 2). Some past researches (Indraratna et al., 1993; Le Pen et al., 2013; Wang et al., 2017) have reported that a small-scaled ballast with the parallel gradation well reproduces the mechanical behavior of the prototype ballast. It is noted that 1/2AB was prepared by the Los Angeles Abrasion (LAA) test using 1/2CB with abrasion time (L) of 50 min (number of turns (N_t) is 1650). The validity of the LAA test for preparing aged ballast can be referred to previous research (Yang et al., 2021). Physical properties of test samples were listed in Table 1.

Table 1 Physical properties of test samples.

Test samples	G_s	ρ_{dmax} (g/cm^3)	ρ_{dm} (g/cm^3)	D_{cm} (%)	w_{opt} (%)	D_{50} (mm)	U_c (mm/mm)	LL (%)	PL (%)	PI (%)	F_c (%)	k_s (m/s)
1/2CB	2.73	1.652	-	-	3.3	21.4	1.42	*NP*	-	-	0	6.51×10^{-2}

1/2AB	2.73	2.162	-	-	7.5	12.2	384.9	21.4	17.6	3.8	14.6	3.39×10^{-4}
1/1CB	2.70	1.682	1.581	94.0	3.0	40.7	1.33	*NP*	-	-	0	-
1/1AB	2.70	2.185	2.198	101.0	7.8	20.3	-	22.0	16.3	5.7	15.0	-

G_s: specific gravity; ρ_{dmax} and w_{opt} are maximum dry density and optimum water content, obtained from compaction E-b method (JGS 0711-2009); ρ_{dm}: in-situ measured dry density; D_{cm}: in-situ measured degree of compaction; D_{50}: mean grain size; U_c: uniformity coefficient; *LL*, *PL*, and *PI*, are liquid limit, plastic limit, and plasticity index, respectively, obtained from test method for liquid and plastic limit of soils (JGS 0141-2009); *NP*: non-plastic; F_c: fine fraction content, means the percentage by weight of ballast material passing the 0.075 mm sieve; k_s: saturated coefficient of permeability at degree of compaction (D_c) of 94% for 1/2CB, and 101% for 1/2AB, fitted by the results of saturated permeability tests with different D_c (Yang et al., 2021).

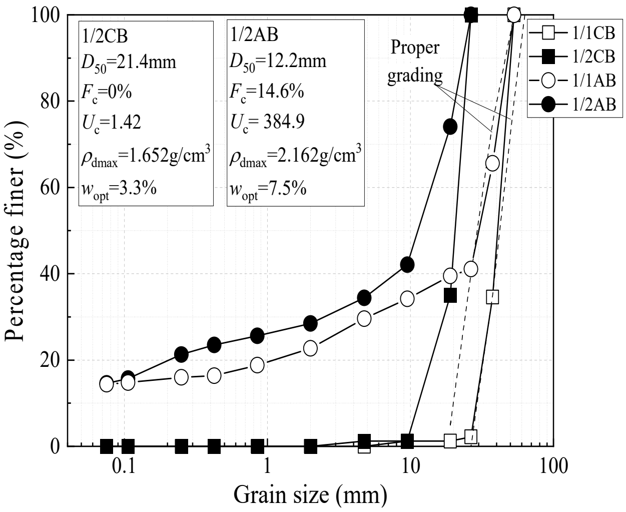

Fig. 2. Grain size distributions of test samples.

In general, fresh ballast is a free draining material with large voids. However, the infiltration of fouling material reduces the voids and restricts water drainage. Indraratna et al. (2010) proposed the Void Contaminant Index (*VCI*) to quantitatively evaluate the degree of fouling for fouled ballast, which can consider the differences in void ratio, specific gravity, and gradation between the fresh ballast and the fouling material.

$$VCI = \frac{(1+e_f)}{e_b} \times \frac{G_{sb}}{Gsf} \times \frac{M_f}{M_b} \times 100 \quad (1)$$

where, e_b, G_{sb}, and M_b are void ratio, specific gravity, and dry mass of fresh ballast, respectively; e_f, G_{sf}, and M_f are void ratio, specific gravity, and dry mass of fouling material, respectively. Based on this definition, Fig. 3 shows the relationships between the *VCI* and F_c or N_t of 1/2AB. It should be noted that in addition to the 1/2AB used in this study, 1/2AB with three other different F_c was also prepared by the LAA tests with different N_t to examine the effectiveness of the LAA test for reproducing the lightly or heavily aged ballast with different F_c

or *VCI*. Here, a lightly or heavily aged ballast refers to the difference in the aging level. For example, 1/2AB (F_c = 6%) is considered a lightly aged ballast, and 1/2AB (F_c = 15%) is considered a heavily aged ballast. Regarding the calculation parameters of *VCI*, the specific gravities (G_{sb}, G_{sf}) of fresh ballast and fouling material are the same. Besides, the e_f and M_f of fouling material with different LAA test times can be calculated by assuming that the initial dry mass of 1/2CB placed into the LAA test instrument is the same as the dry mass of 1/2AB regardless of abrasion time, and that the dry mass of fouling material for 1/2AB is the same as the dry mass of the F_c for 1/2AB with the same abrasion time. As can be seen in Fig. 3(a), *VCI* of 1/2AB is about 32.8%, and it increases approximately linearly with the increase of F_c. Besides, *VCI* also shows an overall increasing trend as the N_t increases (Fig. 3(b)).

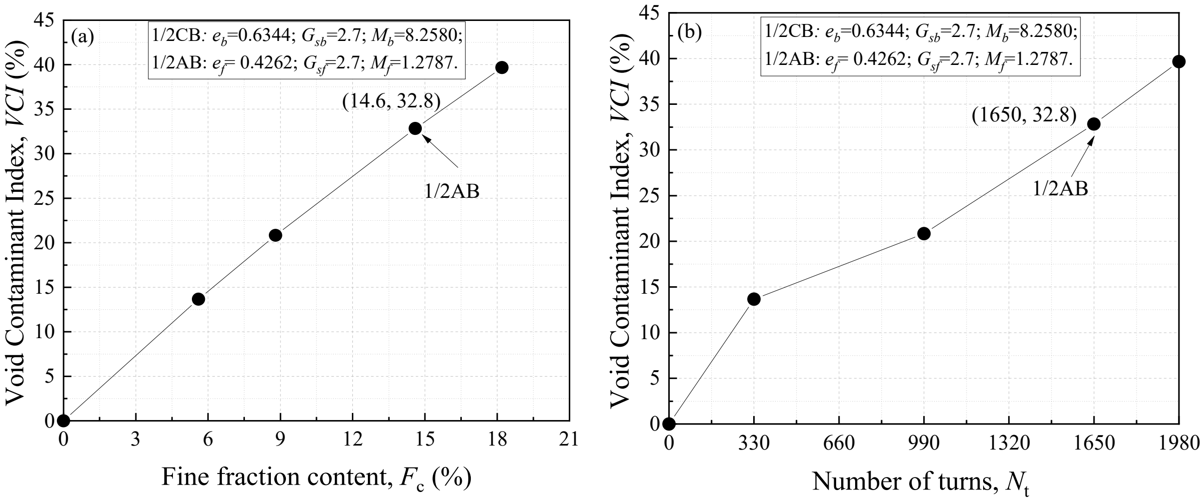

Fig. 3. Relationship between *VCI* and F_c, N_t: (a) *VCI*-F_c; (b) *VCI*- N_t.

3 Test method for cyclic loading triaxial compression test

The cyclic loading triaxial compression (CL) test was performed by a medium-size triaxial apparatus (Fig. 4). The pressure membrane method was adopted in CL tests for unsaturated specimens to apply the matric suction (s). Here, s is defined as $s = u_a - u_w$, u_a is pore air pressure, and u_w is pore water pressure. As for more information about this triaxial apparatus, Ishikawa et al. (2014) and Yang et al. (2021) can be referred. The preparation method of a cylindrical specimen (H = 300 mm, D = 150 mm) in this test was as follows: an air-dried sample (1/2CB, w = 1.69%; 1/2AB, w = 2.01%) was put into the mold in five layers step by step. Each layer was compacted by the vibrator to achieve the targeted D_c values similar to the actual track conditions shown in Table 1. It is worth noting that according to field investigations, the measured D_c of aged ballast in the field condition is close to or even greater than the maximum D_c obtained from the compaction E-b method.

In E-B method, the number of compacted layers for a test sample was 3 layers, and each layer was dropped 92 times through a rammer (rammer mass is 4.5 kg) with the drop height of 450 mm. In this case, a larger D_c (i.e., D_c = 101% for 1/2AB) in the laboratory element test than the maximum D_c can be obtained by controlling the vibration time of the sample. The uniformity of a specimen was ensured because the variations in the initial dry density of the same sample were less than 1%. The test conditions of the CL tests in this study were shown in Table 2. As shown in Table 2, CL tests were performed under three different water contents (air-dried, unsaturated (s = 5 kPa), and saturated) according to the standards of Japanese Geotechnical Society (JGS 0523-2009; JGS 0524-2009; JGS 0527-2009). It is noted that the s of 5 kPa was selected under the unsaturated condition because results of water retention tests (Fig. 5) showed that the water content of the two test samples hardly decreases when the s was greater than 5 kPa. Besides, the effective confining pressure (σ'_c) or net normal stress (σ_{net}) of 20 kPa was selected in CL test, which was referred to that in monotonic loading triaxial compression (ML) test as shown in Table 3 (Yang et al., 2021). Here, σ_{net} is defined as $\sigma_{net} = \sigma_c - u_a$ (σ_c: confining pressure), and the σ_{net} under the unsaturated condition was similar to the σ'_c ($\sigma'_c = \sigma_c - u_a$) under the air-dried condition or σ'_c ($\sigma'_c = \sigma_c - u_w$) under the saturated condition. More importantly, the σ'_c or σ_{net} in CL tests was close to the effective overburden pressure of the typical ballasted track in field conditions (Indraratna et al., 2013b; Suiker et al., 2005).

Table 2 Test conditions and results of CL tests.

Sample	Drainage condition	Water content	σ'_c, σ_{net} (kPa)	ρ_{dc} (g/cm^3)	D_c (%)	S_r (%)	$\varepsilon_{p,\,max}$ (%)
1/2CB	CD test	Air-dried	20.0	1.571	95.1	4.22	1.08
1/2CB	CD test	Unsaturated (s = 5 kPa)	20.0	1.539	93.2	10.62	2.97
1/2CB	CD test	Saturated	20.0	1.541	93.3	100	3.53
1/2AB	CD test	Air-dried	20.0	2.220	101.6	21.7	0.65
1/2AB	CD test	Unsaturated (s = 5 kPa)	20.0	2.198	100.6	67.2	6.40
1/2AB	CD test	Saturated	20.0	2.205	100.9	100	12.09
1/2AB	CU test	Air-dried	20.0	2.196	100.5	21.3	0.97
1/2AB	CU test	Unsaturated (s = 5 kPa)	20.0	2.195	100.5	68.5	8.24
1/2AB	CU test	Saturated	20.0	2.199	100.6	100	Failed

Table 3 Test conditions and results of ML tests (Yang et al., 2021).

Sample	Drainage condition	Water content	σ'_c, σ_{net} (kPa)	ϕ' (deg.)	c', c (kPa)
1/2CB	CD test	Air-dried	20.0, 40.0	58.9	0
1/2CB	CD test	Unsaturated (s = 5 kPa)	20.0, 40.0	55.3	1.6
1/2CB	CD test	Saturated	20.0, 40.0	55.3	0
1/2AB	CU test	Air-dried	20.0, 40.0	59.4	5.1
1/2AB	CU test	Unsaturated (s = 5 kPa)	20.0	49.5	9.4
1/2AB	CU test	Saturated	20.0, 40.0	49.5	4.8

σ'_c is the effective confining pressure under air-dried and saturated conditions; σ_{net} is the net normal stress in unsaturated condition; ϕ' is the effective friction angle; c' stands for effective cohesions under saturated and air-dried conditions; c stands for total cohesion under unsaturated condition, which is composed of two parts: one is the effective cohesion (c') of the saturated soil, and the other is related to the matric suction, as shown in Eq. (2) (Fredlund et al., 1978).

$$c = c' + (u_a - u_w)\tan\phi^b \tag{2}$$

where, ϕ^b is the internal friction angle with respect to the matric suction.

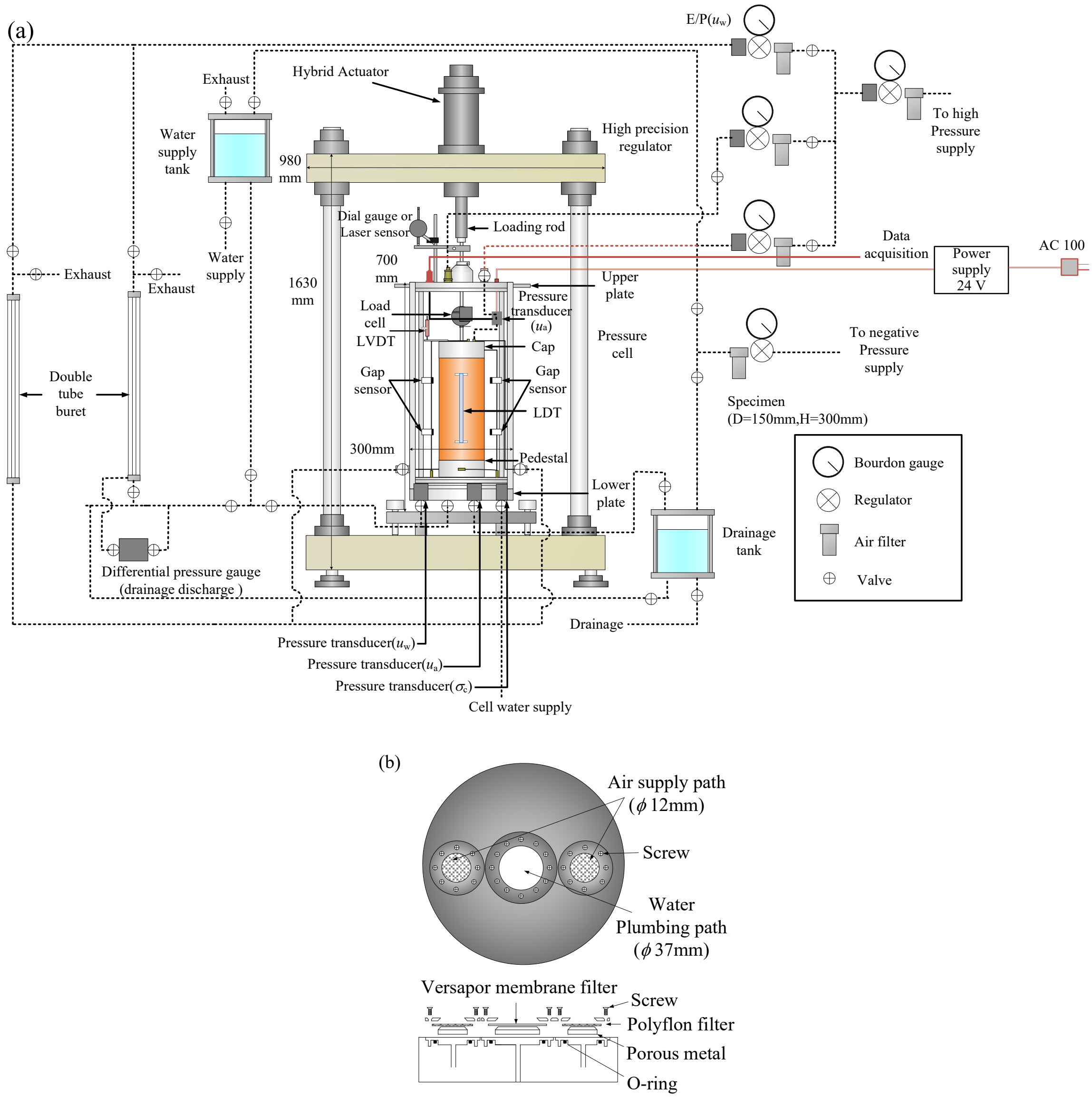

Fig. 4. Medium-size triaxial test apparatus for unsaturated soils: (a) schematic diagram; (b) structures of cap and pedestal (after Yang et al., 2021).

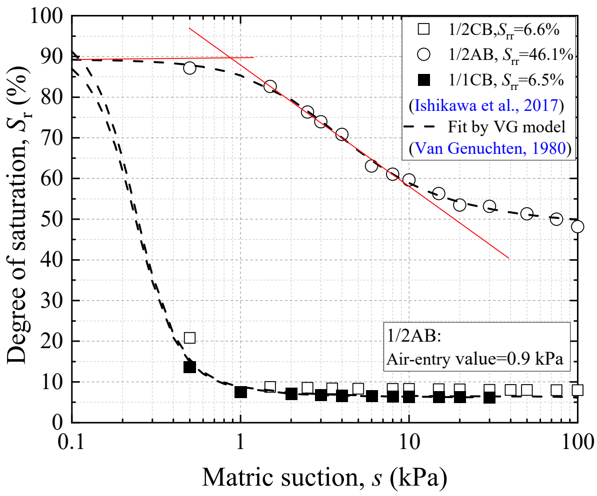

Fig. 5. Soil water characteristic curves of test samples (revised after Yang et al., 2021).

In a CL test, the consolidation process was conducted as follows. Under the air-dried condition, the specimen after the preparation was isotropically consolidated under a designated σ'_c of 20 kPa. Under the saturated condition, the de-aired water was supplied from the bottom end of the specimen, and the pore water pressure (u_w) of 200 kPa was applied to ensure the pore water pressure coefficient B-value was above 0.96. Following the saturation process, the specimen was isotropically consolidated under a specified σ'_c of 20 kPa for 24 hours with σ_c of 220 kPa and the u_w of 200 kPa. Under the unsaturated condition, the de-aired water was immersed from the bottom of the specimen until the initial degree of saturation reached about 90%. Afterwards, the specimen was isotropically consolidated under a prescribed σ_{net} of 20 kPa for 24 hours with σ_c of 220 kPa, pore air pressure (u_a) of 200 kPa, and u_w of 200 kPa. After the consolidation process, an unsaturated specimen with the s of 5 kPa was prepared by reducing u_w while keeping both σ_c and u_a unchanged. Next, the shearing process started after the equilibrium condition was reached in the suction process. The axial deviator stress (σ_d) in sinusoidal waveform ranged from 10 kPa to 80 kPa was cyclically applied to the test specimen of 1/2CB and 1/2AB under the different drainage conditions. In this study, the CL tests for the test specimen of 1/2CB were conducted in CD tests due to its high permeability, while those of 1/2AB were conducted in both CD and CU tests due to its low permeability as shown in Table 1. It is noted that under the unsaturated condition, both pore water and pore air were allowed to drain in the CD test, while both were undrained in the CU test. The number of loading cycles (N_c) in the CL test was 10, 000 or the specimen was failed (permanent axial strain, ε_p>15%), and the loading frequency of 1 Hz was selected by referring to previous research on simulated train loads (Cai et al., 2017; Chazallon et al., 2016).

4 Test results and discussions

4.1 Stress-strain relationship of aged ballast

Fig. 6 and Fig. 7 present the relationships between axial strain (ε_a) and axial deviator stress (σ_d) of 1/2CB and 1/2AB with various water contents at different number of loading cycles (N_c) in CD and CU tests. When other test conditions except the water content are constant, the elastic and plastic strains of both samples increase with the increment of water content. Besides, when comparing stress-strain relationships for both samples in CD tests under unsaturated and saturated conditions, the stiffness of 1/2AB is softer than that of 1/2CB, and the plastic strain rate of 1/2AB is greater than that of 1/2CB, though the stress-strain relationships of both samples are almost similar under air-dried condition. On the other hand, when comparing test results for 1/2AB in CD and CU tests, the difference in the stress-strain relation becomes clear with increasing the water content, and the saturated 1/2AB in the CU test has the largest plastic stain rate. It is worth noting that the stress-strain relationships for unsaturated samples are different in CD and CU tests, since both pore water pressure and pore air pressure change in the CU test due to the fully undrained conditions. In this case, the net normal stress (or effective confining pressure) is not constant in the CU test, while it remains constant in the CD test. Furthermore, as shown in Fig. 6(b), Figs. 7(c) and (d), when comparing the stress-strain relations at different N_c (N_c=10 and 1000), the area of the stress-strain hysteresis curve decreases as the N_c increases, regardless of test samples, water contents, and drainage conditions. More importantly, the changing trend of the stress-strain relationship is more significant for 1/2CB, which indicates that aging changes the development trend of plastic deformation of ballast. These results indicate that the water content, drainage condition, and ballast aging have significant influences on the plastic strain of ballast. As the water content increases, the aged ballast with much fine fraction content and rounded particle shape might reduce the interlock between particles, thereby the lubricating effect of water content and fine fraction content changes the stress-strain relationship of the ballast. Besides, the reduction of σ'_c in CU tests further increases the development of plastic strain, which will be discussed in a later section.

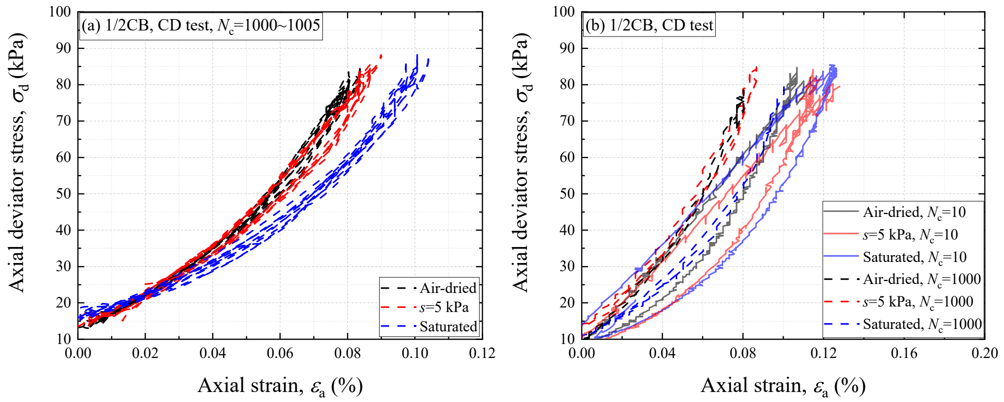

Fig. 6. Stress-strain relationship for 1/2CB with different water contents / N_c in CD tests: (a) N_c =1000~1005; (b) N_c =10 and 1000.

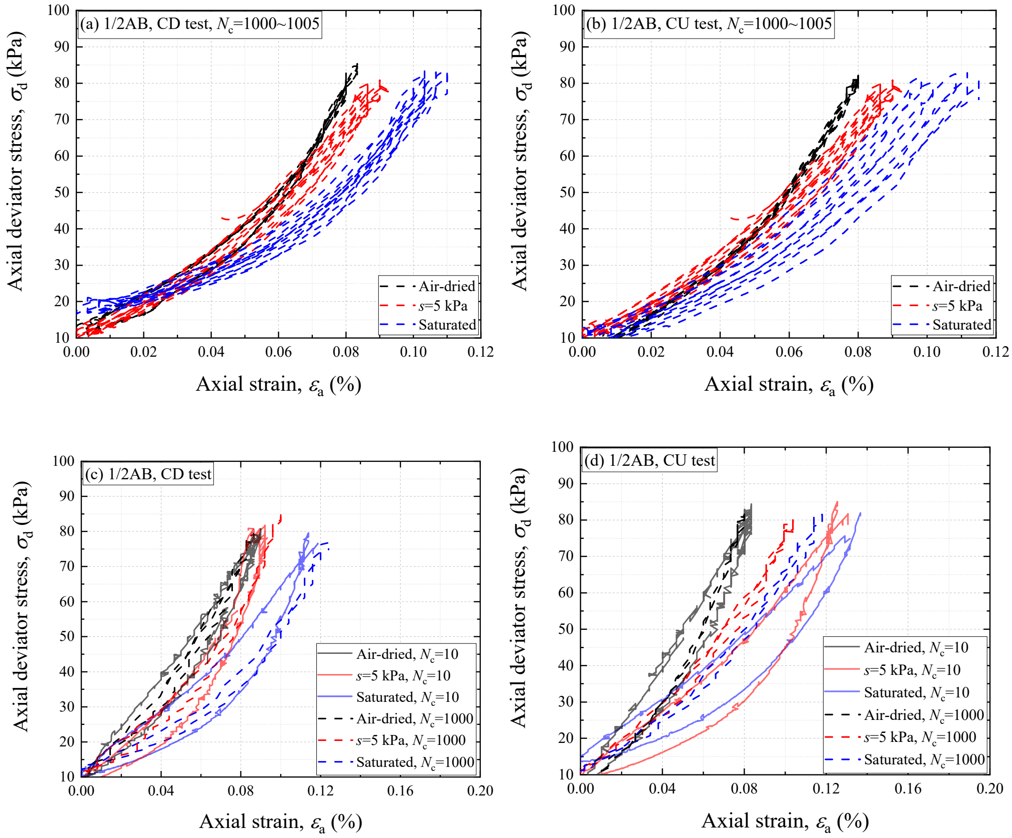

Fig. 7. Stress-strain relationships for 1/2AB with different water contents / N_c in CD and CU tests: (a) CD test, N_c=1000~1005; (b) CU test, N_c=1000~1005; (c) CD test, N_c=10 and 1000; (d) CU test, N_c=10 and 1000.

4.2 Permanent axial deformation behavior of aged ballast

For the plastic deformation of the granular material, the "shakedown theory" (Arnold et al., 2002; Werkmeister et al., 2004; Xiao et al., 2017) was commonly used to describe the plastic deformation and breakage rules of the granular material under cyclic loading. In general, the shakedown behavior of the granular material under cyclic loading includes three stages (Werkmeister et al., 2004): plastic shakedown (steady deformation behavior), plastic creep (failure at a large number of loading cycles), and incremental collapse (failure at a small number of loading cycles), as shown in Fig. 8(a). In addition, Werkmeister et al. (2004) pointed out that the relationship between the plastic strain rate and the plastic strain can be used to distinguish these three types of shakedown behavior, as shown in Fig. 8(b). Region A indicates the plastic shakedown stage, where the plastic strain rate decreases sharply as the plastic strain increases. Region B reveals the plastic creep stage, where the plastic strain rate decreases sharply at first, and then tends to be stable with an increase in plastic strain. Region C indicates the incremental collapse stage, where the plastic strain rate decreases slightly as the plastic strain increases. For the plastic strain rate of railway ballast, previous studies (Mamou et al., 2017; Sun et al., 2019) illustrated that there is a threshold stress level above which significant accumulation of plastic strain and generation of excess pore pressure occurs, especially in undrained conditions. It is noted that Xiao et al. (2017) pointed out that the fresh ballast is generally in a plastic shakedown or plastic creep state after hundreds of loading cycles.

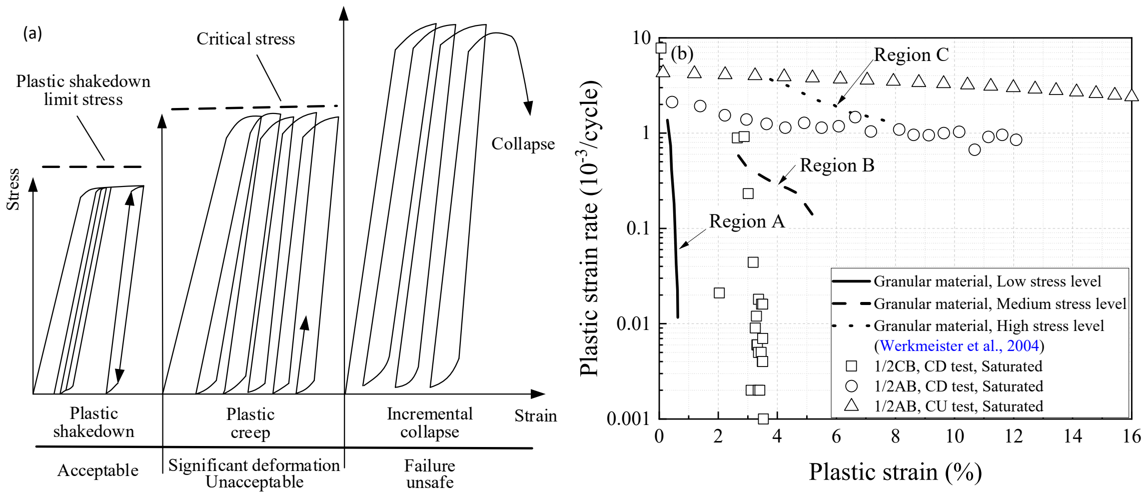

Fig. 8. Typical shakedown behaviors of granular materials under cyclic loading: (a) schematic diagram of the shakedown theory (revised after Werkmeister et al., 2004); (b) relationship between plastic strain rate and plastic strain.

Fig. 9 shows the relationships between the permanent axial strain (ε_p), volumetric strain (ε_v), resilient axial strain (ε_{res}) and number of loading cycles (N_c) up to 10, 000 cycles for test specimens of 1/2CB and 1/2AB with various water contents and drainage conditions. Here, ε_p represents permanent axial strain (cyclic plastic strain) at unloading, and ε_{res} represents the resilient axial strain between the loading and unloading. The ε_p of all specimens shows a rapid growth trend in the initial cyclic loading process, and then the increasing trend of ε_p becomes stable as the N_c increases, irrespective of test conditions. Besides, when comparing the ε_p under the same test conditions except the water content, the ε_p of all specimens increases with the increment of water content, irrespective of test samples. In CD tests for 1/2AB, the ε_p under the air-dried condition shows a stable trend with the increment of N_c, while the ε_p under unsaturated and saturated conditions reveal an approximately linear growth trend with the increment of N_c, as shown in Fig. 9(c). For the dilatancy behavior in CD tests, the volume of unsaturated and saturated specimens is dilated, while the volume of the air-dried specimen is compressed as the ε_p increases with the increment of N_c, irrespective of test samples. The reason for this phenomenon is that the volumes of the fresh and aged ballasts are firstly compressed at axial strain (ε_a) about 1%, followed by dilation with the increase in ε_a during the shear process (Yang et al., 2021). When other conditions are unchanged, the specimen under the higher degree of saturation shows an upward trend in the dilation due to the larger ε_p. Besides, the ε_{res} of both samples in CD tests increases by the sequences in air-dried, unsaturated, and saturated specimens, though the differences in ε_{res} under different water contents are not remarkable as those in the ε_p. Moreover, with the increment of N_c, the ε_{res} shows an increasing trend under the air-dried condition, while it decreases under the unsaturated and saturated conditions. This is because the unsaturated and saturated specimens have larger plastic deformation, which leads to an increase in density and thus greater stiffness. The above results indicate that the permanent/residual axial and volumetric strains of fresh and aged ballast in CD tests are affected by the water content. On the other hand, as shown in Fig. 9(e), the ε_p of 1/2AB under the air-dried condition presents a stable trend with the increment of N_c in CU tests, while ε_p under unsaturated and saturated conditions shows an approximately linear increasing trend with the increment of N_c. It is noted that under the saturated condition, 1/2AB is failed at the N_c of 5, 000 in the CU test. Besides, as shown in Fig. 9(f), ε_{res} in CU tests increases by in the order of air-dried, unsaturated, and saturated specimens. These results indicate that the cyclic plastic deformation of aged ballast is significantly affected by the water content in both CD and CU tests, and the effects of water content on the cyclic plastic deformation are more significant in CU tests.

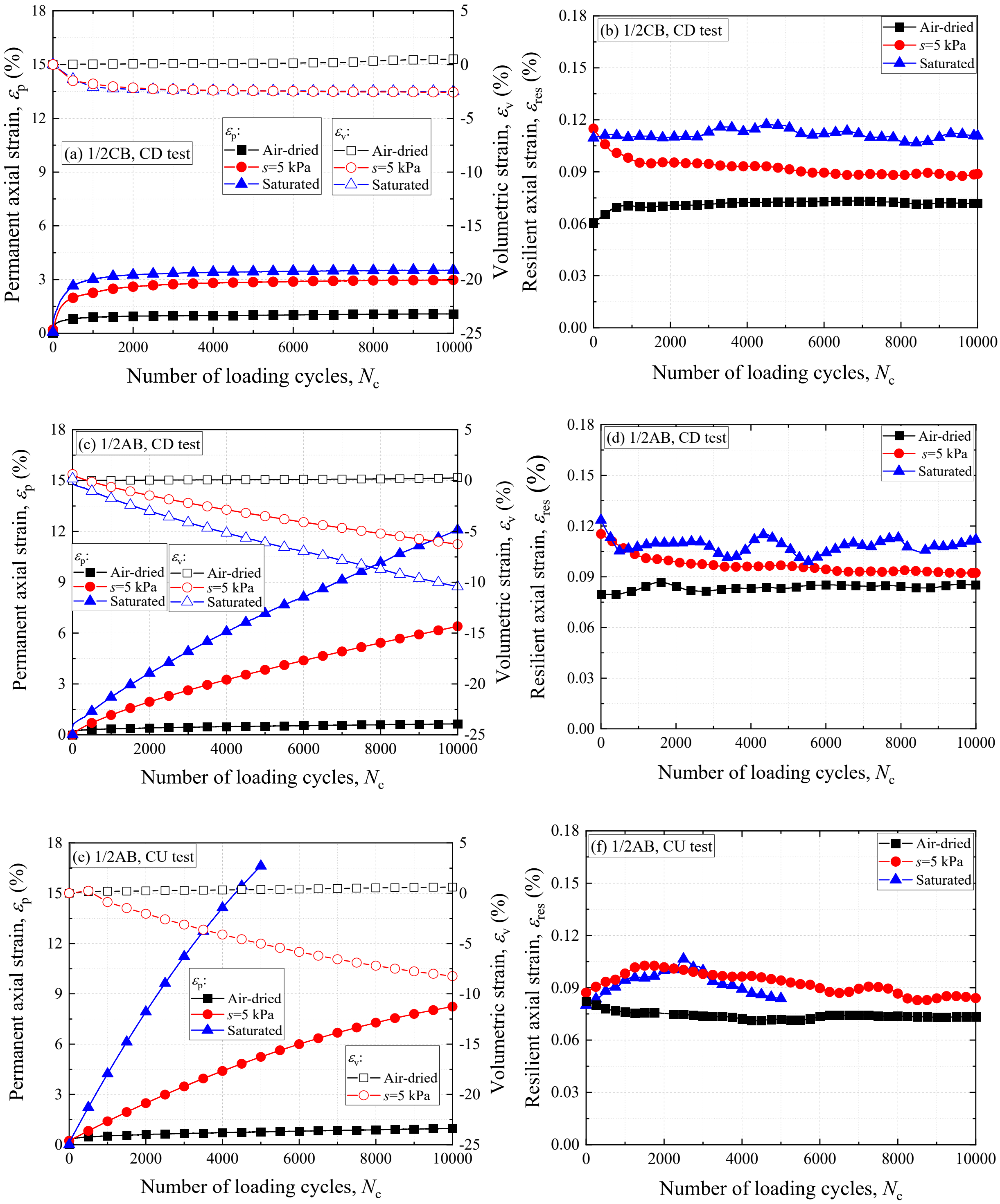

Fig. 9. ε_p, ε_v, and ε_{res} of test samples with different water contents: (a) ε_p and ε_v of 1/2CB in CD tests; (b) ε_{res} of 1/2CB in CD tests; (c) ε_p and ε_v of 1/2AB in CD tests; (d) ε_{res} of 1/2AB in CD tests; (e) ε_p and ε_v of 1/2AB in CU tests; (f) ε_{res} of 1/2AB in CU tests.

4.3 Effects of drainage condition, water content, and aging on permanent axial deformation

4.3.1 Effect of drainage condition

Considering that the drainage condition may affect the permanent axial deformation of aged ballast due to its low permeability, thus both CD and CU tests were conducted for the test specimen of 1/2AB. In this case, Fig. 10(a) shows the comparisons of ε_p for 1/2AB between CD tests and CU tests. The ε_p of 1/2AB in CU tests is larger than those in CD tests, irrespective of water contents. Besides, under the air-dried condition, ε_p of all specimens is small, irrespective of drainage conditions. However, the differences in ε_p under unsaturated and saturated conditions are remarkable between the two types of test conditions, especially under the saturated condition. These findings indicate that in the high degree of saturation condition, the drainage condition has a significant influence on the permanent axial deformation of aged ballast. For a clearer explanation, Fig. 10(b) presents the relationship between the $\varepsilon_{p,\,max}$ and S_e of 1/2AB. Here, $\varepsilon_{p,\,max}$ means the maximum permanent axial strain at N_c of 10, 000, and the effective degree of saturation (S_e) is the normalized water content between the saturated state and the residual degree of saturation (Brooks and Corey, 1964).

$$S_e = \frac{S_r - S_{rr}}{S_{rs} - S_{rr}} \tag{3}$$

where, S_{rs} is the degree of saturation under saturated conditions, and S_{rr} is the residual degree of saturation. It is noted that the S_e of the soil in the air-dried state in this study is considered to be zero. As can be seen in this figure, the $\varepsilon_{p,\,max}$ in CU tests is larger than those in CD tests, regardless of S_e. More importantly, the difference in $\varepsilon_{p,\,max}$ is greater as the water content increases. This indicates that the effect of drainage condition on the permanent axial strain becomes more significant at the higher water content.

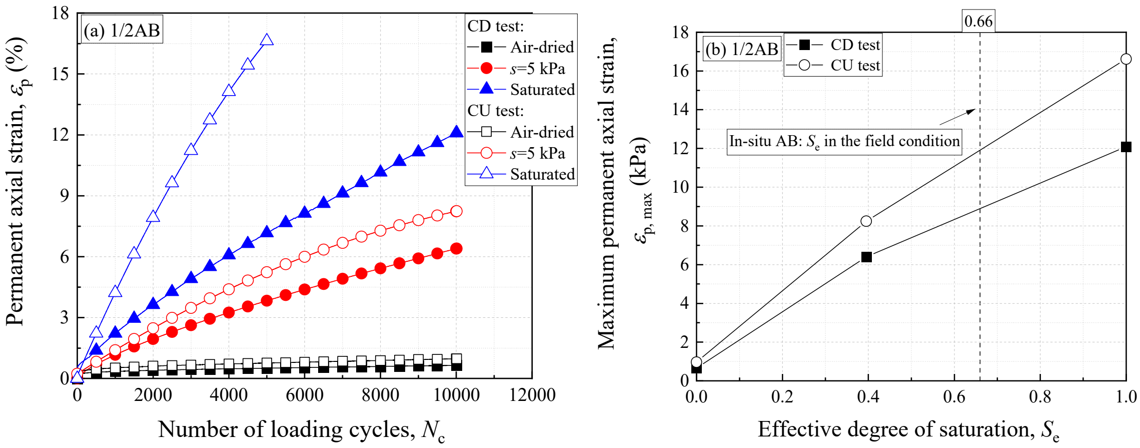

Fig. 10. Comparison of ε_p - N_c and $\varepsilon_{p,\,max}$ - S_e of 1/2AB between CD test and CU test: (a) ε_p - N_c; (b) $\varepsilon_{p,\,max}$ - S_e.

Fig. 11 shows the changes in u_w and ε_p for 1/2AB in CU tests. It is worth mentioning that the increasing trend of excess pore water pressure in the saturated condition is larger than that in the unsaturated condition, which is a probable reason why the saturated specimen is failed at the N_c of 5, 000. It can be inferred that the excess pore water pressure generated in the CU test is one of the factors that affect the permanent axial deformation of the aged ballast. In addition, the water content itself can reduce the shear strength of aged ballast, and induce a greater permanent axial deformation. Besides, the excess pore water pressure shows a whole increasing trend with the N_c, though it shows a downward trend in the initial loading process, irrespective of water content. It is noted that the excess pore water pressure is generated even for the unsaturated sample, since the degree of saturation of 1/2AB under the unsaturated condition is about 70% (Fig. 5). This indicates that due to the low permeability of the heavily aged ballast, the excess pore pressure is easily generated even in an unsaturated state under the repeated train loads, which is consistent with the phenomenon of aged railway tracks under the field condition.

Similar to the increasing trend of excess pore water pressure with the increment of N_c in CU tests, the σ'_c of 1/2AB shows a whole decreasing trend with the increment of N_c, though an increasing trend is observed in the initial loading process, as shown in Fig. 12. To be specific, when the N_c is greater than 500, the σ'_c decreases as the increment of the N_c and the final values of σ'_c in CU tests are smaller than those in CD tests, regardless of water contents. The decrease in σ'_c in CU tests is a reason why the ε_p in CU tests under the same initial test condition is higher than that in CD tests. Besides, the change in σ'_c in CU tests is related to the dilatancy trend of the test specimen. When comparing the final values of σ'_c under different water content conditions, the final value of σ'_c of the saturated specimen is lower than those of unsaturated and air-dried specimens. This is because the positive dilatancy trends become stronger by the sequences in air-dried, unsaturated, and saturated specimens. These results demonstrate that the permanent axial strain of aged ballast is affected by the drainage condition. Considering that the high S_{rr} and low permeability of the aged ballast, the in-situ aged ballast is almost under a partially or fully undrained condition with a high degree of saturation. In general, the cyclic loading tests for fresh and fouled ballasts in an air-dried condition have been carried out in the past researches so far. However, these results indicate that the cyclic loading tests for unsaturated and saturated specimens in partially and fully undrained conditions should be adopted for the accurate estimation of cyclic plastic deformation of heavily aged ballast, though the cyclic loading tests for an air-dried specimen in fully drained condition is suitable for evaluating the permanent deformation of fresh or slightly aged ballast.

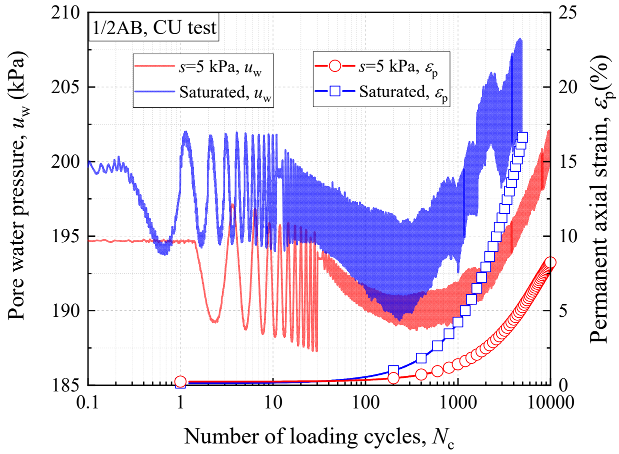

Fig. 11. Changes in pore water pressure/permanent axial strain of 1/2AB in CU tests.

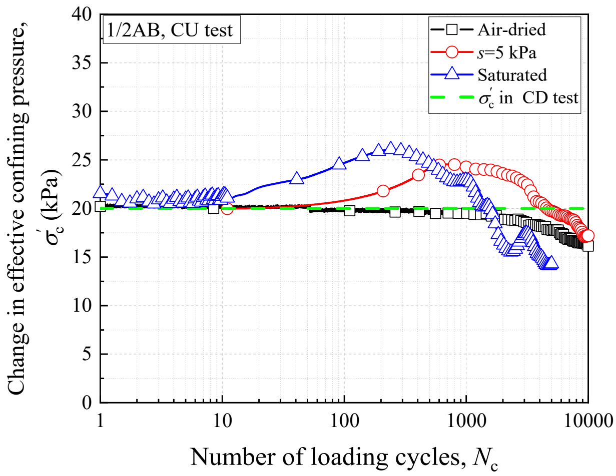

Fig. 12. Changes in effective confining pressure of 1/2AB in CU tests.

4.3.2 Effect of water content

To evaluate the effect of water content on the ε_p, Fig. 13(a) shows the effect of water content on ε_p for both samples in CD tests. When the other initial test conditions are constant except for the water content, the ε_p increases with the increase in water content, irrespective of test samples. Furthermore, the wetting causes aged ballast to increase ε_p dramatically as compared with fresh ballast. As shown in Fig. 13(b), the $\varepsilon_{p,\ max}$ appears a remarkable increasing trend under the higher S_e, regardless of test samples and drainage conditions. These results reveal that the water content has serious influence on permanent axial deformation of both samples, especially for the aged ballast.

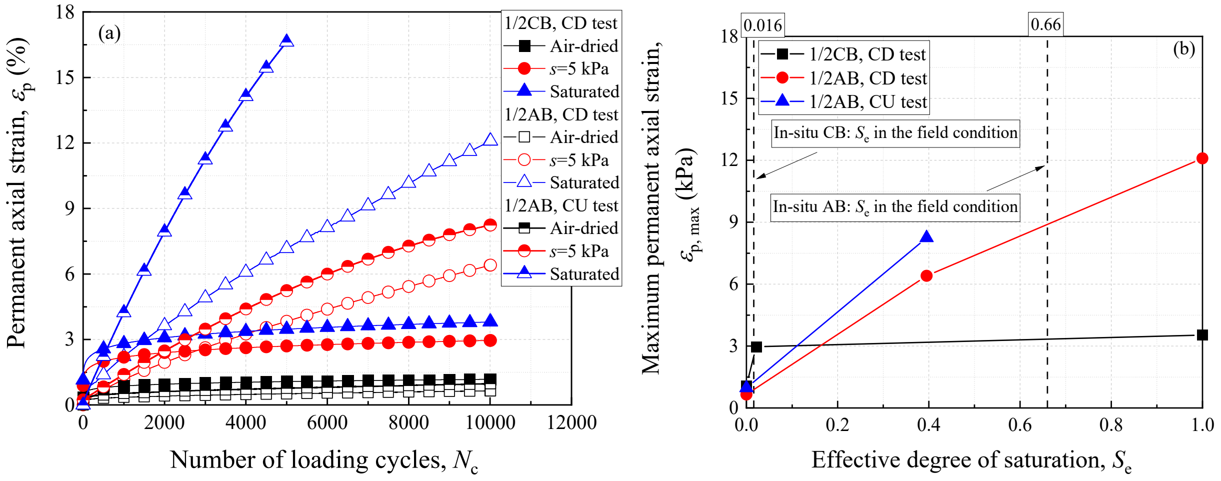

Fig. 13. Effect of water content on ε_p and $\varepsilon_{p, max}$: (a) ε_p - N_c; (B) $\varepsilon_{p, max}$ - S_e.

4.3.3 Effect of aging

As for the effect of aging on the ε_p of ballast, the different tendency of ε_p between fresh and aged ballasts is due to their plastic strain rate being in different "Regions", as shown in Fig. 8(b). It is noted that the plastic strain rate for the fresh and aged ballast was calculated by the increment of plastic strain at each loading cycle during the whole cyclic loading. As illustrated in this figure, the plastic strain rate of the fresh ballast is generally in the Region A, while the plastic strain rate of the aged ballast is generally in the Region B or the Region C. These indicate that the aging significantly changes the tendency of the plastic strain of the ballast from plastic shakedown to incremental collapse stage, though the cyclic stress level of different samples is the same in this study. Furthermore, Fig. 14(a) presents the relationship between the $\varepsilon_{p, max}$ and F_c. As can be seen in this figure, $\varepsilon_{p, max}$ of 1/2AB is higher than those of 1/2CB in unsaturated and saturated conditions, though the opposite trend appears in the air-dried condition. The changing trend of the $\varepsilon_{p, max}$ with various water contents is similar to that of maximum principal stress ratio ($(\sigma_1'/\sigma_3')_{max}$) in the same condition shown in Fig. 14(b) (Yang et al., 2021). These results indicate that the both water content and aging synergistically affect the permanent axial strain of the ballast, and the increase in water content caused by ballast aging negatively enhances the adverse effects on the permanent axial strain. In addition, it should be emphasized that the effects of particle shape changes and increase in fine fraction content on the permanent axial strain of aged ballast are considered simultaneously in this study, though the effect of particle shape changes was not evaluated in previous studies on fouled ballast (Indraratna et al., 2011; Ishikawa et al., 2019). Compared with previous studies, test results in this study indicate that aged ballast has an unexpected smaller permanent axial strain than those of fresh and fouled ballasts in the air-dried condition, while it has a larger permanent axial strain than those of fouled ballast in unsaturated and saturated conditions. The reasonable explanation for this phenomenon is that the smaller and rounder particles produced in the process of ballast breakdown and abrasion might provide a weakening effect in the aggregate matrix by preventing contact between large particles thus greatly reducing the aggregate matrix in the unsaturated and saturated conditions, though the fine particles can also provide a stabilizing effect by filling the voids among larger particles in the air-dried condition. Conclusively, the difference in permanent axial strain between fouled ballast and aged ballast demonstrates that when evaluating the permanent axial strain of aged ballast, it is essential to consider the influence of particle shape, fine fraction content, and water content comprehensively.

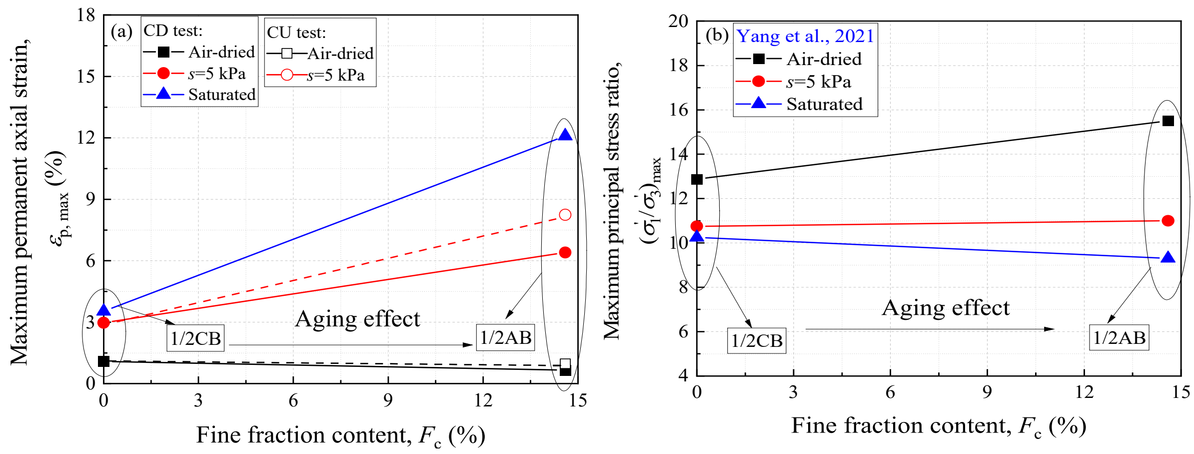

Fig. 14. Effect of aging on $\varepsilon_{p,\,max}$; and $(\sigma_1'/\sigma_3')_{max}$: (a) $\varepsilon_{p,\,max}$; (b) $(\sigma_1'/\sigma_3')_{max}$ (after Yang et al., 2021).

From the above analysis, the results of ML tests and CL tests illustrate that the τ_f and $\varepsilon_{p,\,max}$ are affected by the water content and ballast aging. Thus, the relationships between the $\varepsilon_{p,\,max}$ and τ_f with various water contents and drainage conditions are shown in Fig. 15. As expected, the samples with a lower τ_f appear a higher $\varepsilon_{p,\,max}$, irrespective of test samples and drainage conditions. This indicates that the water content and aging have similar effects on the shear strength and permanent axial strain of ballast, that is the increase in water content or aging might cause a decrease in shear strength and an increase in permanent axial deformation of ballast, and the downward/upward trend of shear strength/permanent axial deformation is more remarkable for aged ballast under the high-water content condition.

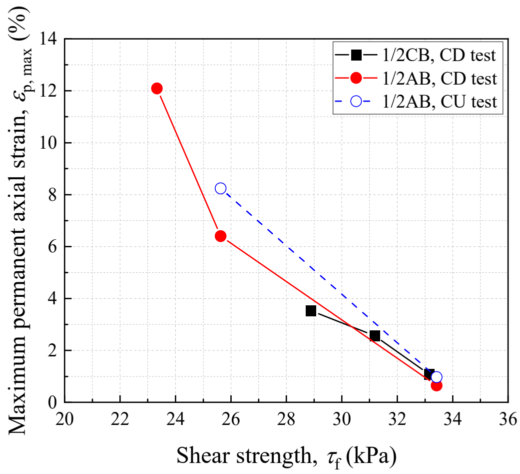

Fig. 15. Relationship between $\varepsilon_{p,\,max}$ and τ_f.

5 Estimation of permanent axial deformation of unsaturated ballast

5.1 Estimation of permanent axial deformation by UIUC model

The UIUC model belongs to a semi-empirical model, and its input parameters can be obtained from ML tests (Qamhia et al., 2016). Therefore, in this section, the applicability of the UIUC model is evaluated by comparing the predicted results by this model with measured results from CL tests. For this model, the permanent axial strain can be calculated as follows:

$$\varepsilon_p = A{N_c}^B \sigma_d^C \left(\frac{\tau_f}{\tau_{max}}\right)^D \quad (4)$$

where, ε_p is the permanent axial strain corresponding to N_c applications (%); σ_d is the axial deviator stress (kPa); A, B, C, D are regression parameters. Besides, τ_f and σ_f are the applied effective shear stress and applied effective normal stress acting on failure plane calculated by Eq. (5) and Eq. (6), respectively; τ_{max} is the maximum effective shear stress at σ_f calculated by Eq. (7) determined by ML tests.

$$\tau_f = \sqrt{\left(\frac{\sigma_d}{2}\right)^2 - \left(\sigma_f - \left(\sigma_3' + \frac{\sigma_d}{2}\right)\right)^2} \quad (5)$$

$$\sigma_f = \frac{2\sigma_3' + 2\tan^2\phi'\sigma_3' + \sigma_d + \tan^2\phi'\sigma_d - \sqrt{\tan^2\phi'\sigma_d^2 + \tan^4\phi'\sigma_d^2}}{2(1+\tan^2\phi')} \quad (6)$$

$$\tau_{max} = c + \sigma_f \tan\phi' \quad (7)$$

where σ_3' is the minimum effective principal stress, which is equal to σ_c' in CL tests; *c* stands for total cohesions of both samples with different water contents, as shown in Table 3. It is noted that the *c* of test samples in air-dried and saturated conditions is equal to the effective cohesion (c').

The input parameters and the corresponding regression parameters of UIUC model for 1/2CB and 1/2AB are shown in Table 4 and Table 5, respectively. It is noted that the input parameters of *c* and ϕ' for 1/2CB were determined by CD tests, while *c* and ϕ' for 1/2AB are determined by CU tests. The regression parameters in Table 5 were obtained by fitting the results of CL tests at different water contents for each test sample. As shown in Table 5, 1/2AB has the higher *A* and *D* values than those of 1/2CB. It means that the aged ballast shows a higher initial permanent axial deformation, and that the effect of (τ_f/τ_{max}) on permanent axial strain becomes more pronounced for the aged ballast as compared with fresh ballast. These indicate that it is feasible to predict the permanent axial strain of fresh and aged ballasts with various water contents by the UIUC model.

Table 4 Input parameters of UIUC model.

Input Parameters	1/2CB	1/2CB	1/2CB	1/2AB	1/2AB	1/2AB
	Air-dried, CD test	*s*=5 kPa, CD test	Saturated, CD test	Air-dried, CD test	*s*=5 kPa, CD test	Saturated, CD test
σ_d (kPa)	80	80	80	80	80	80
σ_f (kPa)	25.77	27.11	27.11	25.57	29.58	29.58
τ_f (kPa)	20.69	22.77	22.77	20.36	25.98	25.98
c (kPa) (Yang et al., 2021)	0	1.6	0	5.1	9.4	4.8
ϕ' (deg.) (Yang et al., 2021)	58.9	55.3	55.3	59.4	49.5	49.5
τ_{max} (kPa)	42.64	40.73	39.16	48.34	44.04	39.44
τ_f/τ_{max}	0.485	0.559	0.581	0.421	0.590	0.659

Table 5 Regression parameters of UIUC model.

Sample	Drainage condition	Regression parameters				
		A	*B*	*C*	*D*	R^2
1/2CB	CD test	0.1938	0.1306	1.2130	6.5239	0.9801
1/2AB	CD test	0.3162	0.6843	0.1066	7.5684	0.9960
1/2AB	CU test (S)	0.3162	0.6843	0.1066	7.5684	-
1/2AB	CU test (D)	0.6020	0.6266	0.1022	6.8378	0.9397

CU test (S) and CU test (D) mean that the same and different regression parameters from CD tests were adopted in CU tests.

Fig. 16 compares the measured and estimated permanent axial strains of 1/2CB with various water contents. The estimated values by the UIUC model using the same regression parameters (Table 5) are consistent with measured values even though the water contents are different. This indicates that the effect of water content on permanent axial deformation of fresh ballast can be effectively estimated by UIUC model. Then, in order to evaluate the applicability of this model to the prediction for the permanent axial deformation of aged ballast,

Fig. 17 compares the measured and estimated permanent axial strains of 1/2AB with different water contents and drainage conditions. It is noted that the regression parameters of 1/2AB are different from those of 1/2CB as shown in Table 5. In addition, the input parameters of σ_d, τ_f, and τ_{max} in Eq. (4) in CU tests are changed due to the change in the σ_3', which can be calculated by the Eqs. (5) ~ (7). Subsequently, the permanent axial strain ($\varepsilon_{p,i}$) at different $N_{c,i}$ in CU tests can be calculated with different $\sigma_{d,i}$, $\tau_{f,i}$, and $\tau_{max,i}$ by Eq. (8). The reason for the fluctuation of the predicted values seen in Fig. 17(b) is that the input parameters of $\sigma_{d,i}$, $\tau_{f,i}$, and $\tau_{max,i}$ are changed as the σ_3' changes in CU tests, while these input parameters are constants adopted for the estimation of CD tests (Table 4).

$$\varepsilon_{\mathrm{p,i}} = \varepsilon_{\mathrm{p,i-1}} + A\left(N_{\mathrm{c,i}}\right)^{B} \sigma_{\mathrm{d,i}}^{C} \left(\frac{\tau_{f,\mathrm{i}}}{\tau_{\mathrm{max,i}}}\right)^{D} - A\left(N_{\mathrm{c,i-1}}\right)^{B} \sigma_{\mathrm{d,i}}^{C} \left(\frac{\tau_{f,\mathrm{i}}}{\tau_{\mathrm{max,i}}}\right)^{D} \tag{8}$$

where, $N_{c,i}$ represents the N_c is ith; $N_{c,i-1}$ represents the N_c is (i-1)th; $\varepsilon_{p,i}$ is the permanent axial strain at the $N_{c,i}$; $\varepsilon_{p,i-1}$ is the permanent axial strain at the $N_{c,i-1}$; $\sigma_{d,i}$, $\tau_{f,i}$, and $\tau_{max,i}$ are the axial deviator stress, effective shear stress, and effective shear strength at the $N_{c,i}$. It can be seen that the estimated permanent axial strains of 1/2AB by UIUC model are consistent with measured values in CD tests (Fig. 17(a)), irrespective of water contents, while the estimated values are different from measured values in CU tests (Fig. 17(b)). The possible reason is that the UIUC model cannot reproduce the effect of the change in excess pore water pressure (Fig. 11) caused by cyclic loading in CU test on the mechanical behavior of ballast. On the other hand, when using different regression parameters from those for CD tests, the estimated values by the UIUC model are consistent with measured values in air-dried and unsaturated conditions, though the estimated value is smaller than the measured value in the saturated condition, as shown in Fig. 17(c). These results prove that the permanent axial deformation of fresh and aged ballasts with various water contents in CD tests can be well estimated by UIUC model by using the same regression parameters, while the applicability of UIUC model to the prediction for permanent axial deformation of aged ballast may be limited in CU tests, since it is difficult to predict the change in excess pore pressure under cyclic loading.

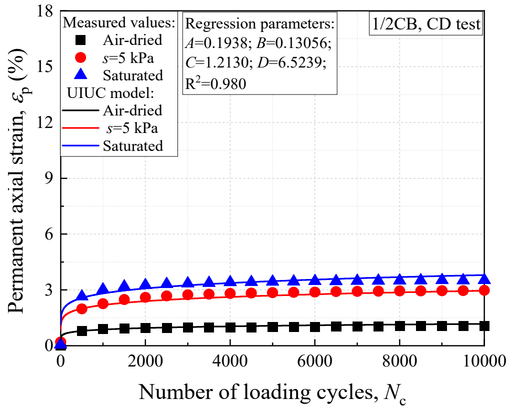

Fig. 16. Comparison of ε_p for 1/2CB with various water contents in CD tests.

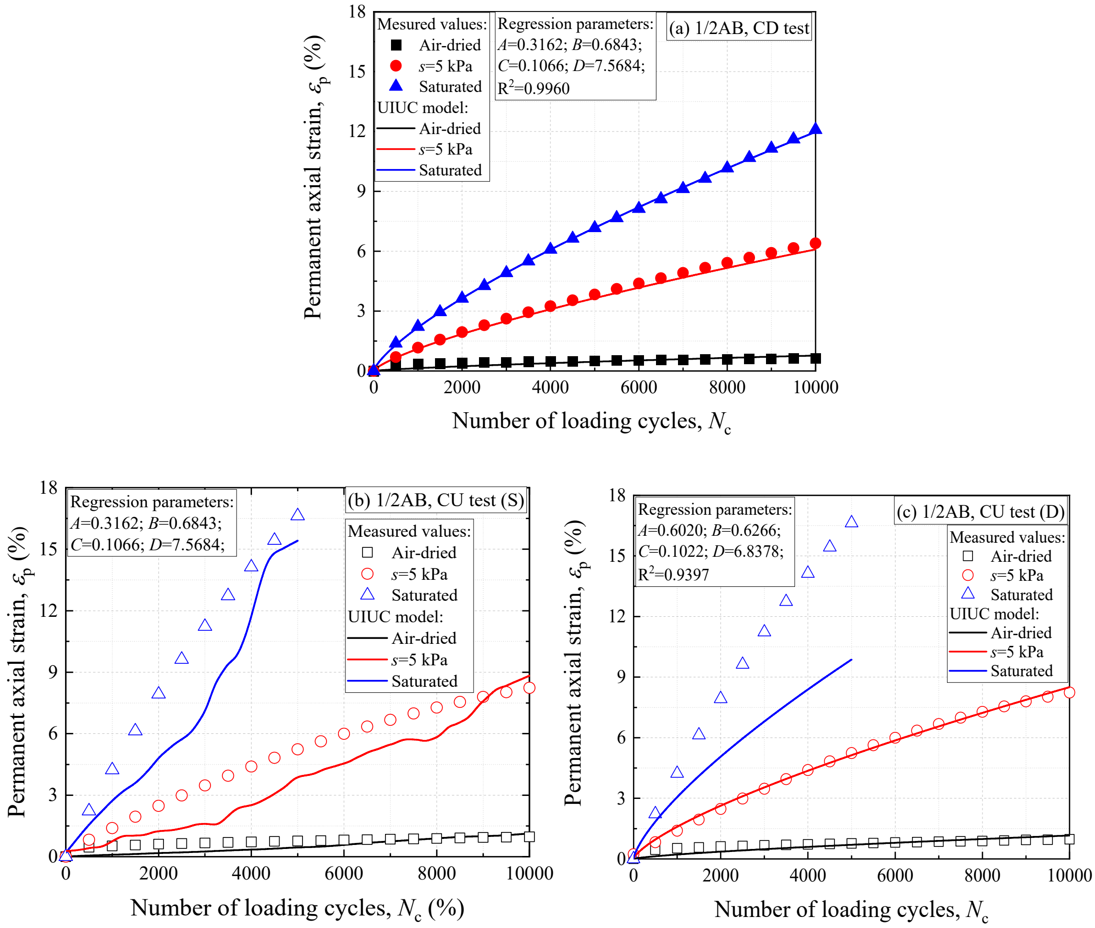

Fig. 17. Comparison of ε_p for 1/2AB with various water contents: (a) CD test; (b) CU test (S); (c) CU test (D).

5.2 Estimation of permanent axial deformation by SSE model

The reliability of the SSE model is discussed by comparing the results of CL tests for fresh and aged ballasts under various water contents with the numerical results. The input parameters of SSE model for 1/2CB and 1/2AB under various water contents and drainage conditions were listed in Table 6. Here, the σ_c' can be determined from the CL test. F_0 can be determined from the ML test (Wood, 1990). μ can be determined from the ML test (Qi et al., 2020). ϕ' can be obtained from the ML test. λ and κ can be determined from the isotropic compression test, which refers to previous study on air-dried ballast (Okayasu et al., 2014). In accordance with observations reported in Alonso et al. (1990), λ depends on the matric suction (s), which can be determined from CL tests. Besides, p_i, $U(R)$, $U(Re)$, and R_e are material constants independent on water content, while R_{emax} changes depending on the water content, all of which can be fitted by the results of CL tests.

Table 6 Input parameters of SSE model.

Sample	1/2CB	1/2CB	1/2CB	1/2AB	1/2AB	1/2AB
Drainage condition	CD test			CD test, CU test		
Water content	Air-dried	s=5 kPa	Saturated	Air-dried	s=5 kPa	Saturated
σ_c'	20	20	20	20	20	20
F_0	1078	887	842	1186	895	792
μ	0.3	0.3	0.3	0.3	0.3	0.3
ϕ'	58.9	55.3	55.3	59.4	49.5	49.5
λ	0.05	0.07	0.09	0.05	0.07	0.09
κ	0.0005	0.0005	0.0005	0.0005	0.0005	0.0005
p_i	45	45	45	45	45	45
$U(R)$	20	20	20	150	150	150
$U(R_e)$	4	4	4	25	25	25
R_e	0.001	0.001	0.001	0.001	0.001	0.001
R_{emax}	0.150	0.067	0.060	0.047	0.037	0.022

σ_c' is the effective confining pressure; F_0 is an initial value of the size of the normal yield surface; μ is the Poisson ratio; λ and κ are the slopes of the normal-consolidation and swelling line; p_i, $U(R)$, and $U(R_e)$ are material constant; R_e is a ratio of the size of the elastic boundary surface to the size of the normal-yield surface; R_{emax} is the maximum value of the R_e.

Fig. 18 compares the permanent axial strain of 1/2CB with various water contents between simulations and tests. It can be found that the predicted values by SSE model are consistent with measured values, regardless of water contents. These results prove that the applicability of the SSE model to the prediction for the permanent axial deformation of fresh ballast by considering the effect of water content.

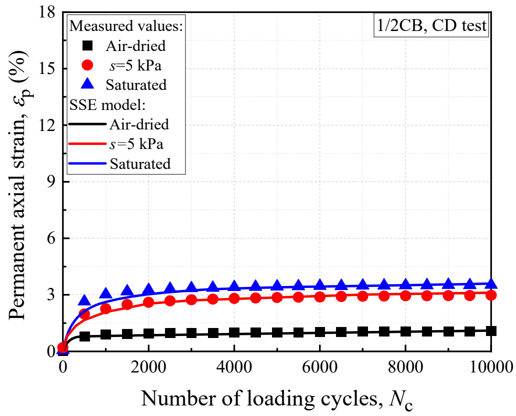

Fig. 18. Comparison of ε_p for 1/2CB in CD tests between simulations and tests.

On the other hand, Fig. 19 compares the simulated and measured permanent axial strains of 1/2AB in different drainage conditions. As can be seen in Fig. 19(a), the permanent axial strains of 1/2AB with various water contents in CD tests can be well predicted by SSE model. However, as shown in Fig. 19(b), there is a certain difference between the estimated and measured permanent axial strain of 1/2AB in CU tests, and with increasing S_r, the difference becomes larger due to the generation of excess pore water pressure. This is because only a mechanical model in numerical simulations is adopted in this study, which causes the SSE model cannot accurately predict the change in excess pore water pressure under cyclic loading. These results prove that the SSE model can well predict the permanent axial deformation of fresh and aged ballasts with various water contents in CD tests, and there is a possibility for improving the prediction accuracy of the SSE model for aged ballast in CU tests by employing a hydro-mechanical model.

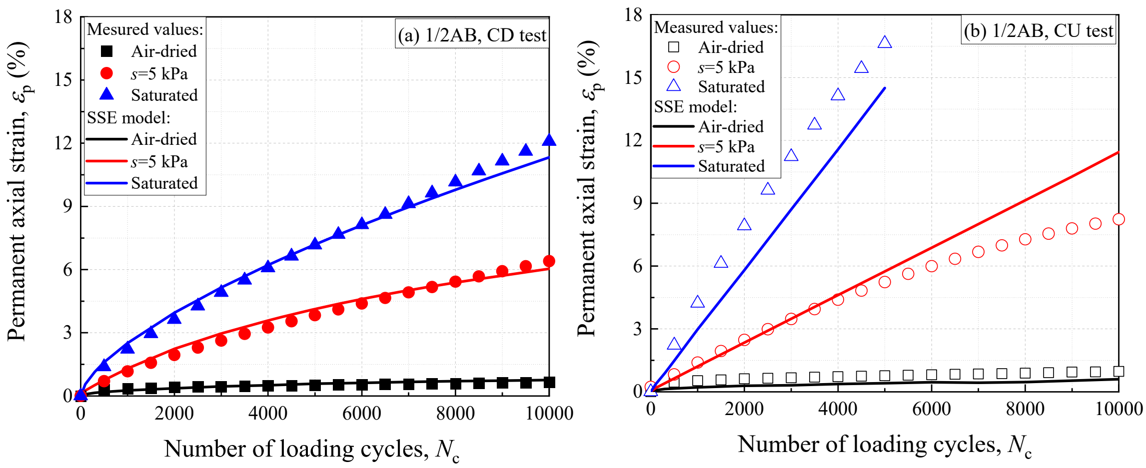

Fig. 19. Comparisons of ε_p for 1/2AB between simulations and tests: (a) CD test (b) CU test.

To analyze the influence of water content on input parameters of SSE model for both samples, the changes in normalized input parameters with the effective degree of saturation (S_e) for 1/2CB and 1/2AB are shown in Fig. 20. It is noted that this figure only plots input parameters that change with S_e, instead of all input parameters. Here, the value of each input parameter of 1/2CB in the air-dried condition is taken as the standard value, and the values of normalized input parameters under various test conditions are the ratio of original values to standard values. It shows that the F_0 decreases with the increase in water content, regardless of test samples. As for the $U(R)$, $U(R_e)$ and R_e, they are unchanged with various water contents, regardless of test samples. Besides, the R_{emax} decreases with the increment of S_e, irrespective of test samples and drainage conditions. As for the ϕ' in the unsaturated condition, Fredlund et al. (1978) proposed that an increase in matric suction (s) results in an increase in the apparent cohesion while maintaining the same ϕ' as the saturated soils. In this case, when other test conditions are constant, the ϕ' maintains constant, even though the S_e changes, except in the air-dried condition. Moreover, as the S_e increases, the λ increases while the κ does not change, which is consistent with the results of Alonso et al. (1990). On the other hand, previous study (Yang et al., 2021) revealed that the S_e of the fresh ballast is generally below 0.016 and the S_e of the aged ballast is generally above 0.66 in the field conditions. In this case, the input parameters of the fresh ballast under the air-dried condition can reproduce actual conditions for a new railway line, while the input parameters of the aged ballast under the saturated condition can simulate actual conditions for an old railway line since when the S_e is greater than 0.66, the normalized input parameters of the aged ballast show a small change with the water content.

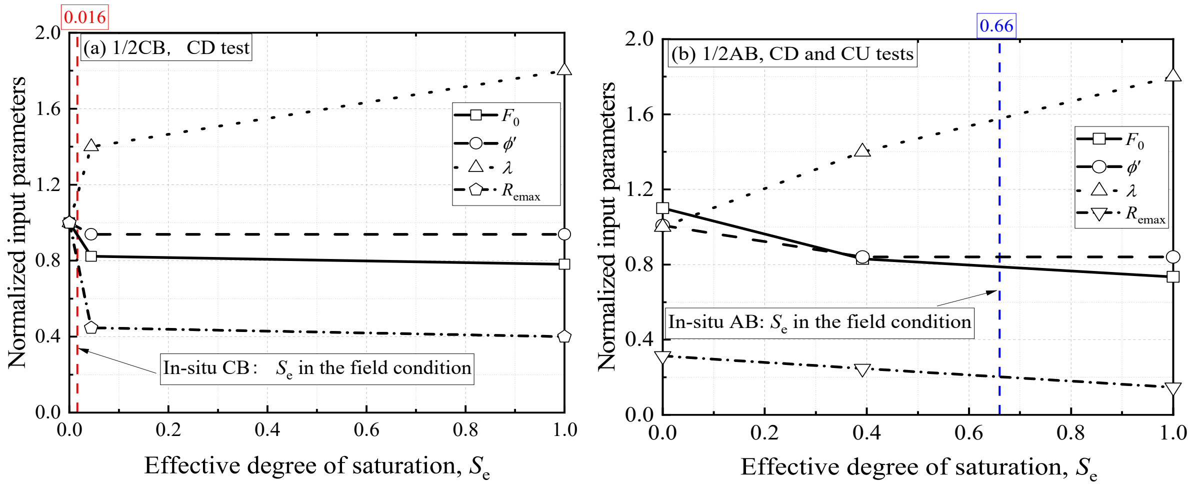

Fig. 20. Relationship between normalized input parameters and S_e of test samples: (a): 1/2CB in CD tests; (b) 1/2AB in CD and CU tests.

6 Conclusions

In this study, the influence of aging on cyclic plastic deformation of unsaturated ballast was evaluated by performing a series of the CL tests. After that, the applicability of the UIUC model and the SSE model was verified to the prediction for the cyclic plastic deformation of unsaturated ballast by considering aging effects. The following findings can be mainly obtained:

- The permanent axial deformation of ballast increases with the increase in water content, irrespective of test samples and drainage conditions, and wetting has a more significant impact on the permanent axial deformation of aged ballast as compared with fresh ballast. It can be inferred that the water content and aging effect synergistically affect the permanent axial deformation of ballast, and this is the reason why the aged ballast with a high degree of saturation would appear a greater permanent axial deformation than that of fresh ballast with a low degree of saturation at the field condition.

- For the aged ballast, the permanent axial deformation in CU tests is larger than that in CD tests, regardless of water contents. Besides, the effect of drainage conditions on the cyclic plastic deformation for aged ballast becomes more significant as the degree of saturation increases since the excess pore water pressure increases significantly at higher degree of saturation.
- The shear strength and permanent axial deformation are affected by the water content and aging. When other test conditions are constant, the unsaturated ballast with the lower shear strength in the monotonic loading condition has the higher permanent axial deformation in the cyclic loading condition, irrespective of test samples and drainage conditions. The decreasing/increasing trend of shear strength/permanent axial deformation is more remarkable, in case of both the water content and fine fraction content increase.
- Aged ballast has smaller permanent axial strain than that of fouled ballast under the air-dried condition, while it has a larger permanent axial strain than that of fouled ballast under unsaturated and saturated conditions. Thus, the difference in permanent axial strain between fouled ballast and aged ballast demonstrates that when evaluating the permanent axial strain of aged ballast, it is essential to consider the influence of particle shape, fine fraction content, and water content comprehensively.
- In CD tests, the influence of water content on the permanent axial deformation of fresh and aged ballasts can be well estimated by the UIUC model with the same regression parameters, even though water contents are different. However, in CU tests, the applicability of the UIUC model to the prediction for the permanent axial deformation of aged ballast is limited, since it is difficult to predict the change in excess pore pressure under cyclic loading.
- The SSE model can well predict the permanent axial deformation of fresh and aged ballasts with different water contents in CD tests. Thus, the input parameters of the fresh ballast under the air-dried condition can reproduce actual conditions for a new railway line. On the other hand, the effect of water content on the permanent axial deformation of aged ballast in CU tests could not accurately predict by the SSE model, since a mechanical model was adopted in this study. However, the input parameters of the aged ballast under the

saturated condition may simulate actual conditions for an old railway line when the hydro-mechanical analysis is adopted.

The findings of this research indicate that it is necessary to consider the effects of the drainage condition and water content on the hydro-mechanical behavior of the aged ballast, due to the low permeability and high residual degree of saturation. For the fresh ballast, the air-dried specimen in triaxial tests under the fully drained condition can reproduce the actual conditions. However, for the aged ballast, the unsaturated and saturated specimens in triaxial tests under partially and fully undrained conditions can reproduce the actual conditions. Therefore, for the actual design, when evaluating the cyclic plastic deformation of the aged ballast, it is important to first consider the hydraulic properties (i.e., permeability and water retentivity), and select appropriate test conditions (i.e., CD and CU tests) based on these properties. For example, when the fine fraction content of aged ballast exceeds a threshold (i.e., F_c>15) or when the coefficient of permeability of aged ballast is less than a threshold (i.e., k_s<10^{-4}), the undrained test conditions should be selected. Besides, the UIUC model is suitable for predicting the permanent axial deformation of fresh ballast or slightly aged ballast under the drained condition, and the SSE model shows good potential to estimate the permanent axial deformation of fresh and aged ballasts under different drainage conditions when the hydro-mechanical analysis is adopted, although the applicability of the SSE model in this study is verified only based on the mechanical analysis under the drained condition. However, the findings in this study were obtained under limited test conditions (only one unsaturated state, fine fraction content, and confining pressure). Further laboratory element tests (triaxial compression test, water retention test, and permeability test) considering more different degrees of saturation, fine fraction contents, and confining pressures need to be conducted in the future to investigate the hydro-mechanical behavior of aged ballast, and to further determine the threshold value between heavily and sightly aged ballast. More importantly, the applicability of the UIUC model and the SSE model to the prediction for the permanent axial deformation of aged ballast in the undrained condition still needs further study.

Acknowledgement

This research is a part of the Joint Research with Railway Technical Research Institute, and this research was supported in part by Grant-in-Aid for Scientific Research (B) (19H02234) and (A) (16H02360) from Japan

Society for the Promotion of Science (JSPS) KAKENHI. This research was realized with financial support from the China Scholarship Council.

References

Abadi T, Le Pen L, Zervos A, Powrie W. A review and evaluation of ballast settlement models using results from the Southampton Railway Testing Facility (SRTF). In Proceeding of the 3rd International Conference on Advances in Transportation Geotechnics, Guimaraes, Portugal, 4-7 September 2016: 999-1006.

Alonso EE, Gens A, Josa A. A constitutive model for partially saturated soils. Geotechnique 1990; 40(3): 405-430.

Arnold G, Dawson A, Hughes D, Robinson, D. The application of shakedown approach to granular pavement layers. In Proceedings of the 9th International Conference on Asphalt Pavements, August 2002: Copenhagen (Vol. 1).

Brooks RH, Corey AT. Hydraulic properties of porous media. Hydrology Paper. Colorado State University; No. 3. Fort Collins, CO;1964.

Chazallon C, Hornych P, Mouhoubi S. Elastoplastic model for the long-term behavior modeling of unbound granular materials in flexible pavements. Int J GeoMech 2016;6(4):279–89.

Cai YQ, Guo L, Jardine RJ, Yang ZX, Wang J. Stress–strain response of soft clay to traffic loading. Geotechnique 2017;67(5):446–51.

Chow LC, Mishra D, and Tutumluer E. Framework for development of an improved unbound aggregate base rutting model for mechanistic-empirical pavement design. Transportation Research Record: Journal of the Transportation Research Board, 2014a; 2401, 11-21.

Chow LC, Mishra D, and Tutumluer E. Aggregate base course material testing and rutting model development. Final Report, NCDOT Project 2013-18, December; 2014b.

Dareeju B, Gallage C, Dhanasekar M, and Ishikawa T. Effects of particle size distribution in the response of model granular materials in multi-ring shear. In International Conference on Geotechnical Engineering ICGE Colombo, Colombo, Sri lanka, 2015; 10-11.

Ebrahimi A, Tinjum JM, Edil TB. Deformational behavior of fouled railway ballast. Can Geotech J 2015; 52(3): 344–355.

Fredlund DG, Morgenstern NR, Widger RA. The shear strength of unsaturated soils. Can Geotech J 1978; 15(3): 313–321.

Habiballah T, Chazallon C. An elastoplastic model based on the shakedown concept for flexible pavements unbound granular materials. International Journal for Numerical and Analytical Methods in Geomechanics, 2005; 29: 577-596.

Hashiguchi K, Ueno M. Elastoplastic constitutive laws of granular materials. Constitutive Equations of Soils (Proc. 9th Int. Conf. Soil Mech. Found. Eng., Spec. Ses.9), Tokyo, JSSMFE, 73-82, 1977.

Indraratna B, Wijewardena LSS, Balasubramaniam AS. Large-scale triaxial testing of greywacke rockfill. Géotechnique,1993; 43(1):37-51.

Indraratna, B, Nimbalkar, S, Tennakoon, N, 2010. The behavior of ballasted track foundations: track drainage and geosynthetic reinforcement. In: Fratta, D., Puppala, A., Muhunthan, B. (Eds.), GeoFlorida 2010: Advances in Analysis, Modeling & Design (GSP 199), pp. 2378–2387.

Indraratna B, Su L, Rujikiatkamjorn C. A new parameter for classification and evaluation of railway ballast fouling. Can Geotech J 2011;48(2):322–326.

Indraratna B, Ngo NT, Rujikiatkamjorn C. Deformation of coal fouled ballast stabilized with geogrid under cyclic load. J Geotech Geoenvironmental Eng 2013a; 139: 1275–1289.

Indraratna B, Tennakoon N, Nimbalkar S, Rujikiatkamjorn C. Behavior of clay-fouled ballast under drained triaxial testing. Géotechnique 2013b;63(5):410–419.

Ishikawa T, Zhang Y, Tokoro T, Miura S. Medium-size triaxial apparatus for unsaturated granular subbase course materials. Soils Found 2014; 54(1): 67–80.

Ishikawa T, Matsutani S, Tokoro T, Nakamura T, Momoya Y. Influence of parallel grading on hydro-mechanical characteristics of unsaturated fouled ballast. The 10th International Conference on the Bearing Capacity of Roads, Railways and Airfields, Athens, Greece, 1817–25; 2017.

Ishikawa T, Lin TS, Yang JQ, Tokoro T, Tutumluer E. Application of the UIUC model for predicting ballast settlement to unsaturated ballasts under moving wheel loads. Transp Geotech 2019; 18: 149–162.

Iwan WD. On a class of models for the yielding behavior of continuous and composite systems. Journal of Applied Mechanic, 1967; 34(3): 612-617.

Japanese Geotechnical Society. Test method for liquid limit and plastic limit of soils (JGS 0141-2009). Japanese Geotechnical Society Standards Laboratory Testing Standards of Geomater 2009; 1:1–8.

Japanese Geotechnical Society. Method for consolidated-undrained triaxial compression test on soils with pore water pressure measurements (JGS 0523-2009). Japanese Geotechnical Society Standards Laboratory Testing Standards of Geomater 2009; 1: 1–9.

Japanese Geotechnical Society. Method for consolidated-drained triaxial compression test on soils (JGS 0524-2009). Japanese Geotechnical Society Standards Laboratory Testing Standards of Geomater 2009; 1: 1–8.

Japanese Geotechnical Society. Method for triaxial compression test on unsaturated soils (JGS 0527-2009). Japanese Geotechnical Society Standards Laboratory Testing Standards of Geomater 2009; 2:1–13.

Japanese Geotechnical Society. Test method for soil compaction using a rammer (JGS 0711–2009). Japanese Geotech Soc Standards Laboratory Testing Standards Geomater 2009;1:1–10.

Le Pen L, Powrie W, Zervos A, Ahmed S, Aingaran S. Dependence of shape on particle size for a crushed rock railway ballast. Granular Matter, 2013; 15(6): 849-861.

Lekarp F, Isacsson U, and Dawson A. State of the art. II: Permanent axial strain response of unbound aggregates. Journal of Transportation Engineering, 2000; 126(1), 76-83.

Lackenby J, Indraratna B, McDowell G, Christie D. Effect of confining pressure on ballast degradation and deformation under cyclic triaxial loading. Géotechnique, 2007; 57(6), 527-536.

Monismith, CL, Ogawa N, and Freeme CR. Permanent deformation characteristics of subgrade soils due to repeated loading. Transportation Research Record, 537, 1975.

Mroz Z, Norris V, Zienkiewicz O. An anisotropic, critical state model for soils subject to cyclic loading. Géotechnique, 1981; 31(4): 451-469.

Mamou A, Powrie W, Priest JA, Clayton C. The effects of drainage on the behaviour of railway track foundation materials during cyclic loading. Géotechnique, 2017; 67(10): 845-854.

Niemunis A, Wichtmann T, Triantafyllidis T. A high-cycle accumulation model for sand. Computers and Geotechnics, 2005; 32, 245–263.

Qamhia I, Tutumluer E, Chow LC, Mishra D. A framework to utilize shear strength properties for evaluating rutting Potentials of unbound aggregate materials. Procedia Engineering, 2016; 143, 911-920.

Qi S, Cui YJ, Chen RP, Wang HL, Lamas-Lopez F, Aimedieu P, Dupla JC, Canou J, Saussine G. Influence of grain size distribution of inclusions on the mechanical behaviours of track-bed materials. Géotechnique, 2020; 70(3), 238-247.

Okayasu T, Nakamurab T, Muramoto K, Momoya Y. Elastoplastic deformation behavior for ballast under monotonic and cyclic loading conditions. Proceedings of the 18th International Conference of the ISTVS, Seoul, Korea, 2014.

Railway Technical Research Institute (RTRI). Design standard for Railway Structures and Commentary–Track Structures. Tokyo: Maruzen, 2012. (in Japanese)

Selig E, Waters J. Track geotechnology and sub-structure management. London, UK: Thomas Telford; 1994.

Suiker AS, Selig ET, Frenkel R. Static and cyclic triaxial testing of ballast and subballast. J Geotech Geoenvironmental Eng 2005;131(6):771–82.

Sun Q, Indraratna B, Ngo NT. Effect of increase in load and frequency on the resilience of railway ballast. Géotechnique, 2019; 69(9): 833-840.

Tennakoon N, Indraratna, Rujikiatkamjorn C, Nimbalkar S, Neville T. The role of ballast-fouling characteristics on the drainage capacity of rail substructure. Geotechnical Testing Journal 2012; 35(4):629-40.

Tsutsumi S. Toyosada M, Hashiguchi K. Extended subloading surface model incorporating elastic boundary concept, Journal of applied mechanics 2016;9: 455-62.

Van Genuchten MT. A closed-form equation for predicting the hydraulic conductivity of unsaturated soils. Soil Sci Soc Am J 1980; 44, 892–898.

Wood DM. Soil behavior and critical state soil mechanics. Cambridge (UK): Cambridge University Press; 1990.

Werkmeister S, Dawson AR, Wellner F. Pavement design model for unbound granular materials. Journal of Transportation Engineering, 2014; 130(5), 665–674.

Wang HL, Cui YJ, Lamas-Lopez F, Dupla JC, Canou J, Calon N, Saussine G, Aimedieu P, Chen RP. Effects of inclusion contents on the resilient modulus and damping ratio of unsaturated track-bed materials. Canadian Geotechnical Journal, 2017;54(12):1672-1681.

Xiao, J, Zhang D, Wei K, Luo Z. Shakedown behaviors of railway ballast under cyclic loading. Construction and building materials, 2017:155, 1206-1214.

Yang JQ, Ishikawa T, Lin TS, Tokoro T, Nakamura T, and Momoya Y. Influence of aging on hydromechanical behavior of unsaturated ballast. Transportation Geotechnics 2021:27, 100480.